Low Temperature Materials

AFOSR
Final Technical Report
Air Force Contract No. F49620-91-C-0044

March 1994

Submitted to
Air Force Office of Scientific Research
Air Force Systems Command
Bolling Air Force Base
Washington, DC 20332-6448

MARTIN MARIETTA

Submitted by
MARTIN MARIETTA LABORATORIES • SYRACUSE
Syracuse, NY 13221

DISCLAIMER NOTICE

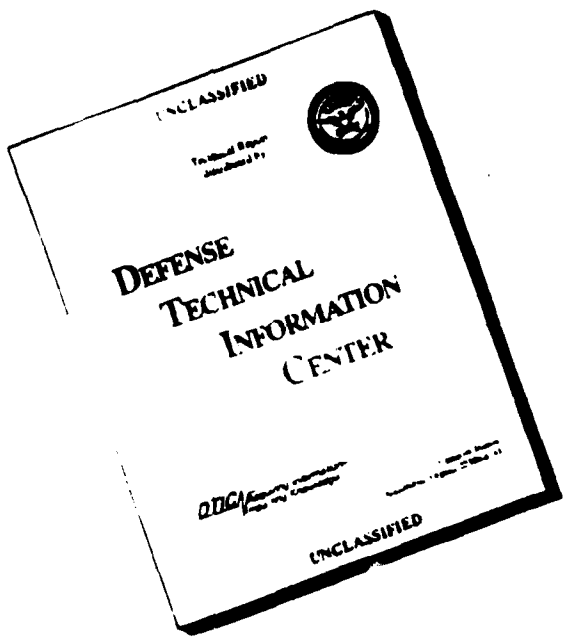

THIS REPORT IS INCOMPLETE BUT IS THE BEST AVAILABLE COPY FURNISHED TO THE CENTER. THERE ARE MULTIPLE MISSING PAGES. ALL ATTEMPTS TO DATE TO OBTAIN THE MISSING PAGES HAVE BEEN UNSUCCESSFUL.

UNCLASSIFIED

SECURITY CLASSIFICATION OF THIS PAGE

REPORT DOCUMENTATION PAGE

Form Approved OMB No. 0704-0188

1a. REPORT SECURITY CLASSIFICATION

1b. RESTRICTIVE MARKINGS

2a. SECURITY CLASSIFICATION AUTHORITY

3. DISTRIBUTION/ AVAILABILITY OF REPORT Approved for public release; distribution unlimited. unlimited

2b. DECLASSIFICATION/ DOWNGRADING SCHEDULE

4. PERFORMING ORGANIZATION REPORT NUMBER(S)

5. MONITORING ORGANIZATION REPORT NUMBER(S)
AFOSR-TR- 94 0231

6a. NAME OF PERFORMING ORGANIZATION
Martin Marietta Laboratories • Syracuse

6b. OFFICE SYMBOL (If applicable)

7a. NAME OF MONITORING ORGANIZATION
Air Force Office of Scientific Research

6c. ADDRESS (City, State, and ZIP Code)
P.O. Box 4840 EP3
Syracuse, New York 13221

7b. ADDRESS (City, State, and ZIP Code)
Building 410
Bolling Air Force Base, DC 20332-6448

8a. NAME OF FUNDING/ SPONSORING ORGANIZATION
Air Force Office of Scientific Research

8b. OFFICE SYMBOL (If applicable)
NE

9. PROCUREMENT INSTRUMENT IDENTIFICATION NUMBER
F49620-91-C-0044

8c. ADDRESS (City, State, and ZIP Code)
Building 410
Bolling Air Force Base
Washington DC 20332-6448

10. SOURCE OF FUNDING NUMBERS

PROGRAM ELEMENT NO.	PROJECT NO.	TASK NO.	WORK UNIT ACCESSION NO.
61102F	2305	BS	

11. TITLE (Include Security Classification)
Low Temperature Materials

12. PERSONAL AUTHOR(S)
J.M. Ballingall, P. Ho, J. Mazurowski, L. Lester, K. C. Hwang, S. Gupta, Tom Rogers, J. Whitaker, H. Hwang

13a. TYPE OF REPORT	13b. TIME COVERED	14. DATE OF REPORT (Year, Month, Day)	15. PAGE COUNT
Final Technical	FROM 6/91 TO 1/94	1994, March	

16. SUPPLEMENTARY NOTATION

17. COSATI CODES			18. SUBJECT TERMS (Continue on reverse if necessary and identify by block number)
FIELD	GROUP	SUB-GROUP	Epitaxy, AlGaAs-InGaAs-GaAs, Pseudomorphic heterostructures, strained layer supperlattices, dislocations, photoluminescence, Hall effect, electron diffraction, photoreflectance.

19. ABSTRACT (continue on reverse if necessary and identify by block number)

$In_xGa_{1-x}As$ (x=0.25—0.35) grown at low temperature on GaAs by molecular beam epitaxy is characterized by Hall effect, transmission electron microscopy, and ultrafastoptical testing. As with low temperature (LT) GaAs, the resistivity is generally higher after a brief anneal at 600°C. High-resolution transmission electron micrography shows all the as-grown epilayers grown directly on GaAs to be heavily dislocated due to the large lattice mismatch (2—3%). Annealed layers also show precipitate formation, in addition to the dislocations. Like LT GaAs, $In_xGa_{1-x}As$ lifetimes shorten as growth temperatures are reduced; and LT $In_xGa_{1-x}As$ lifetimes are generally shorter in as-grown samples than in annealed samples. The metal-semiconductor-metal photodetectors we fabricated on the material exhibit response times of 1—3 picoseconds, comparable to results reported on GaAs grown at low temperature, and the fastest ever reported in the wavelength range of 1.0—1.3μm. To improve the crystalline quality and to distinguish detector speed and responsivity limitations due to dislocations versus defects induced by LT growth, we have grown 3μm-thick graded layers of $In_xAl_{1-x}As$ between the GaAs substrates and $In_{0.35}Ga_{0.65}As$ films. The $In_xAl_{1-x}As$ layers are heavily dislocated, with the dislocation density increasing with distance from the GaAs substrate, and abruptly terminating at or below the $In_{0.35}Ga_{0.65}As$ layer. The $In_{0.35}Ga_{0.65}As$ films are generally free of dislocations and electron mobilities are an order of magnitude higher than those of films grown directly on GaAs. Ultrafast optical testing using photoconductively switched coplanar electrodes show equivalent electron lifetimes of 1-3ps for dislocation-free LT $In_{0.35}Ga_{0.65}As$ and LT $In_{0.35}Ga_{0.65}As$ grown directly on GaAs, demonstrating that the short electron lifetimes are caused by LT-induced defects. This correlates with the trend reported by us for LT $In_{0.35}Ga_{0.65}As$ grown directly on GaAs, namely that the electron lifetime decreases with decreasing growth temperature, as also observed for LT GaAs.

20. DISTRIBUTION/ AVAILABILITY OF ABSTRACT
☐ UNCLASSIFIED/ UNLIMITED ☐ SAME AS RPT. ☐ DTIC USERS

21. ABSTRACT SECURITY CLASSIFICATION
Unclass

22a. NAME OF RESPONSIBLE INDIVIDUAL
Dr. Gerald Witt

22b. TELEPHONE (Include Area Code)
(202) 767-4931

22c. OFFICE SYMBOL
NE

DD Form 1473, JUN: 86 Previous editions are obsolete.

UNCLASSIFIED
SECURITY CLASSIFICATION OF THIS PAGE

Table of Contents

List of Figures

List of Tables

Introduction

Ultrafast optoelectronic applications require photoconductors with subpicosecond carrier lifetimes and high resistivity. Subpicosecond carrier lifetimes have previously been achieved by lowering growth temperatures to ≈ 200°C in MBE-grown GaAs epilayers.[1] The semi-insulating nature and high breakdown-voltage of these epilayers also enabled the fabrication of submicron interdigitated photodetectors with the unprecedented bandwidth of 375 GHz and a responsivity of ≈ 0.1A/W.[2] These properties have been attributed to excess As incorporation during low-temperature MBE growth.[3] We assumed therefore that this approach of low-temperature (LT) MBE growth should be applicable to other As-based materials to achieve ultrashort carrier lifetimes.

Because lattice-matched $In_xGa_{1-x}As$ (x=0.53) exhibits a very low resistivity of ≈ 10^{-2} Ωcm, we chose to investigate the growth of $In_xGa_{1-x}As$ ($0.25 \leq x \geq 0.35$) on GaAs to produce higher resistivity epilayers. As with LT GaAs, LT InGaAs resistivity also increased after a brief anneal at 600°C. Transmission electron microscopy (TEM) showed that all the as-grown epilayers grown directly on GaAs were heavily dislocated due to the large lattice mismatch (2-3%). When the layers were annealed, in addition to the dislocations, precipitates also formed. The precipitates were arsenic-rich, though whether these are pure arsenic clusters, as often found in annealed LT GaAs, has not yet been confirmed. To improve the crystalline quality and to distinguish detector speed and responsivity limitations due to dislocations versus defects inducted by LT growth, we grew 3μm-thick graded layers of $In_xAl_{1-x}As$ between the GaAs substrates and $In_{0.35}Ga_{0.65}As$ films. The $In_xAl_{1-x}As$ layers are heavily dislocated, with the dislocation density increasing with distance from the GaAs substrate, and abruptly terminating at or below the $In_{0.35}Ga_{0.65}As$ layer. The $In_{0.35}Ga_{0.65}As$ films are generally free of dislocations and electron mobilities are on order of magnitude higher than those of films grown directly on GaAs.

To ascertain the response of the InGaAs material for high-speed photoconductive detectors, we measured high-temporal-resolution optical reflectivity and switching. Our measurements were used to screen layers for the more time consuming process of metal-semiconductor-metal (MSM) device fabrication. Like LT GaAs, $In_xGa_{1-x}As$ lifetimes shorten as growth temperature is reduced; and lifetimes are generally shorter in as-grown samples than in annealed samples. Ultrafast optical testing using photoconductively switched coplanar electrodes show equivalent electron lifetimes of 1-3ps for dislocation-free LT $In_{0.35}Ga_{0.65}As$ and LT $In_{0.35}Ga_{0.65}As$ grown directly on GaAs, demonstrating that the short electron lifetimes are caused by LT-induced defects. We fabricated MSMs by electron beam lithography with finger-widths and spacings of 2.0, 1.0, 0.5, and 0.2μm. The MSMs were tested with the high-temporal-resolution optical switching measurement. Our results yield the fastest detectors (1-3ps FWHM) ever reported in the 1.0-1.3μm range.

Research Progress

MATERIALS GROWTH

We grew all of the InGaAs material layers in our Varian GEN II MBE system on 3-inch GaAs substrates using indium-free substrate holders. The substrates were LEC semi-insulating (100) ±0.5°. The GaAs native oxide was desorbed in the MBE growth chamber at 600°C under an As_4 flux. Substrate temperatures were reduced to 120° - 300°C for the $In_xGa_{1-x}As$ growth. We used a growth rate of 1.0μm/h with a V/III beam equivalent pressure ratio of 15. Films were grown to thicknesses of 1.0-1.2μm. After layer growth, some layers were annealed in-situ by raising the substrate temperature to 600°C for 15 minutes. Tables I and II summarize the growth and characterization data for layers grown directly on GaAs. Table III summarizes data for layers grown in the dislocation reduction study.

For the dislocation reduction study, layers were grown on a graded InAlAs buffer (~3μm thick). The InAlAs begins on the substrate with a 5% InAs mole franction and is graded up to 35% InAs to match the $In_{0.35}Ga_{0.65}As$. The InAlAs buffers were grown at 550°C (M-1331) and 500°C (M-1334). M-1333 was grown as a control sample. As seen in Table III, electron mobility improves by an order of magnitude with the graded buffers. This is due to a dramatic reduction in dislocation density in the $In_{0.35}Ga_{0.65}As$ as reported in the next section.

Table 1. Growth Data of InGaAs Wafers. x=0.25

Wafer	Growth Temp. (°C)	Anneal	Resistivity Ω-cm	Mobility (cm^2/V-s)	Lifetime (ps)	Responsivity (10^{-5} A/W)	Structure
1251	300	No	$1.6x10^5$	4120	12.5	3.1	Single crystalline, heavily dislocated
1252	300	Yes	$6.8x10^3$	2950	21.0	5.2	Like 1251, with precipates
1623	250	No	$5.5x10^2$	1110	8.0	3.0	Single crystalline, heavily dislocated
1624	250	Yes	$1.4x10^3$	2730	40.0	3.0	Like 1623, with precipitates
1625	200	No	$1.6x10^2$	20	3.0	0.6	Single crystalline, heavily disclocated
1626	200	Yes	$8.8x10^3$	2260	7.3	5.5	Like 1624, with precipitates
1713	160	No	85	8.5	Unmeasurable		High defect content, some twin grains
1714	160	Yes	$4.5x10^4$	4210	2.0	0.4	Like 1713, with precipitates

Table 2. Growth Data of InGaAs Wafers. X=0.35

Wafer	Growth Temp. (°C)	Anneal	Resistivity Ω-cm	Mobility (cm^2/V-s)	Lifetime (ps)	Responsivity (10^{-5} A/W)	Structure
1747	200	No	71	44	Unmeasurable		Epi, high defect content, many twin grains
1748	200	Yes	1320	303	4.0	3.0	Like 1747, with precipitates
1749	160	No	270	91	4.5	0.2	Amorphous with surface "cells" of crystallization
1750	160	Yes	260	894	5.5	2.1	Polycrystalline with near-substrate epi layer, reduced defect content
1751	120	No	$1.8x10^4$	1600	<1.0	0.03	Completely amorphous
1752	120	Yes	77	550	7.0	3.1	Epi w/twins, low defect content

R-11/92-2AT

Table 3. Growth Data of InGaAs Wafers Grown in the Dislocation Reduction Study.

Wafer	Growth Temp. (°C)	Anneal	InAlAs Buffer	Resistivity Ω-cm	Mobility (cm^2/V-s)
M-1331	180	No	Yes	8.9E3	280
M-1333	180	No	No	8.7E3	17
M-1334	180	No	Yes	1.2E4	160

JMB 3/9/94-1

TEM CHARACTERIZATION

Sample Preparation

We scribed and cleaved samples to produce two 4 x12 mm pieces. These pieces were ultrasonically cleaved in methylene chloride and then ethyl alcohol, and dried with compressed air. These pieces were "sandwiched" with similarly cleaned pieces of silicon. Each sample was coated with epoxy (G1 from Gatan, Inc.) and the two pieces from each sample were placed with their LT-InGaAs layers facing each other in the center of the sandwich. The sandwich was

heated to no more than 100°C and held at temperature for ≈15 minutes to cure the epoxy. After slow cooling, 3 mm slices were cut from the sandwich using a wire saw with a diamond-impregnated stainless steel wire. The slices were ground and polished to ≈10 μm thicknesses using a special lapping jig. This new procedure produces thinner, more uniform TEM samples which require minimal ion-beam thinning. Our samples were ion-beam thinned using 4-5 kV at 0.5 mA gun current; the angle of incidence was 20° and we cooled with liquid nitrogen.

We examined all the samples using our JEOL JEM-2010 transmission electron microscope. Operating voltage was 200 kV. X-ray spectra were obtained using a LINK eXL energy dispersive spectrometer system.

TEM Results.

The micrographs and x-ray spectra from Sample 3-1626 (annealed) show results that are representative of all the x=0.25 samples grown at 200°-300°C and then annealed. The average InGaAs layer thickness from twelve measurements using four different magnifications is 1.206+0.005 μm. The boundaries of the layer are not very sharp; some roughness in the free surface and "rough" strain contrast at the GaAs interface are visible. From the bright field micrographs, it is evident that the LT- InGaAs layer has a much greater dislocation density than the substrate. Precipitates are also visible in the LT layer, even at magnifications of 40,000 (see Figure 1).

Figure 2 shows the As-rich nature of the precipitates. The L_α x-ray lines from Ga and As are low energy lines that are strongly affected by absorption and overlap of the absorption edge for In. This causes the intensity of these lines to behave irregularly as a function of sample thickness and matrix (InGaAs) interference. The K_α x-ray lines are not affected by these factors. However lattice fringes in the precipitates (see Figure 3) are measured as 3.30Å which is not an obvious match with any of the pure As phases.

We can summarize the LT InGaAs (x=0.25) layers grown on GaAs substrates from 200-300°C by the following:

- The layers in all samples were epitaxial single crystals with high quality InGaAs interfaces.
- Precipitates were not observed for samples in the as-grown condition.
- The samples subjected to an anneal contained precipitates and these precipitates were not noticeably different for the samples and temperatures examined.
- The precipitates are As-rich, but no conclusive electron diffraction patterns could be obtained matching the precipitates to one of the pure As phases.
- The precipitates are coherent with their InGaAs matrix and their contrast in bright field TEM images is very sensitive to tilt/diffracting condition, which when combined with the observed shapes suggest a very thin disk precipitate.
- All LT layers contained a higher dislocation density than the adjacent GaAs substrate, but the available data cannot substantiate if more dislocations are present in the samples containing precipitates.

Some differences from the above results obtained at 200-300°C were observed as the growth temperature was lowered to 160°C. For example, Sample 3-1713, grown at 160°C, has planar defects along the <111> directions in the fcc InGaAs crystal which appear to be very fine "micro" -twins (Figure 4). The surface of the layer is somewhat rough, showing some topography due to the twins emerging at the surface. A few boundaries extend through the LT layer normal to the substrate and appear to separate very large twin-oriented grains or domains. Some of these latter boundaries may simply be low-angle grain boundaries.

The structure of Sample 3-1714, which was grown at 160°C and then annealed, is not very different from Sample 3-1713. The number of boundaries extending through the layer normal to the substrate is larger (see Figure 5) and these "macroscopic" twin domains in the LT-layer give characteristic twin diffraction patterns (see Figure 6). The density of the micro-twin within a given domain appears reduced. As-rich precipitates are also in this sample, and some are substantially larger than those seen up to this point (see Figure 7).

As we approached x=0.35, the crystalline structure of our samples became more varied. Sample 3-1747 (grown at 200°C) was predominantly epitaxial with many twin related grains or domains, as was seen in 3-1713 and 3-1714. The higher density of the macro-twin domains gives this sample a more columnar grain appearance (Figure 8).

Sample 3-1748, grown at 200°C and annealed, is very similar to 3-1747 and bears the same relationship to 3-1747 as 3-1714 does to 3-1713—i.e., a smaller concentration of micro-twin defects and As-rich precipitates. We noted that there are large equiaxed grains near the surface of the LT layer, which could have resulted from a recrystallizing during the anneal.

Sample 3-1749 (grown at 160°C) has different regions of crystalline structure. The layer is mostly amorphous, and has a number of polycrystalline "cells" at the surface which appear to have crystallized into the amorphous material (note boundary curvature in Figure 9). The layer is thickest where there is the most polycrystalline surface material, which may indicate some significant difference in density between amorphous and crystalline material. The polycrystalline cells have a structure very much like that of Sample 3-1747.

Sample 3-1750, grown at 160°C and annealed, has three regions demarcated: first, a near-substrate epi-region; second, a predominate, large, equiaxed grain center region; and third, a smaller, equiaxed grain surface region (shown in Figure 10). We saw no evidence of precipitates in the polycrystalline regions. We could not ascertain if any precipitates are in the highly strained and defective epi-layer, but none stands out clearly. X-ray information from the epi layer did not indicate any As-rich precipitates

Sample 3-1751 (grown at 120°C) is the most uninteresting from a microstructural standpoint because it is completely amorphous. Such amorphousness is totally absent in Sample 3-1752 which was grown at 120°C and annealed. The anneal produced a crystalline layer without the high defect density found in previous samples as was indicated by their diffraction patterns. No images were observed that led us to believe there are precipitates in this sample.

Figure 24 shows the InGaAs/GaAs interface. It can be seen that there is a region 10 - 30 nm in width in the InGaAs at the interface of defect-free material before the twinning begins.

Sample M-1334: The results from this sample are shown in Fig. 25. Again, these images have many similarities to the M-1331 series. In M-1334, the LT InGaAs layer can be seen to be free of defects. The dislocation densities in the InAlAs layers of M-1331 and M-1334 appear similar. The primary difference between the M-1331 and M-1334 samples is in the dislocation-free 0.2 μm layer at the top of the InAlAs layer. In sample M-1334, defects are seen in this layer that were not present in M-1331. While the contrast from these defects is complex, they appear to be inclined stacking faults. These faults terminate at the InAlAs/InGaAs interface, and appear to originate near where the dislocations end in the InAlAs layer. It is interesting to note that there is some contrast in the LT InGaAs layer, normal to the interface, at locations corresponding to these faults in the InAlAs (see Fig. 26). This appears to be a form of strain contrast, and the presence of these faults may create additional strain in the LT layer.

Another dislocation Burgers vector set yielded contrast characteristics for the dislocations consistent with 1/2[10-1] or 1/2[01-1] 60° type II dislocations, as seen for M-1331.

OPTICAL TESTING AND DEVICE RESULTS

Time-Resolved Reflectivity

Two types of optical tests were used by the Ultrafast Science Laboratory at the University of Michigan. The first is all-optical, time-resolved reflectivity measurement. This is quick and contactless, which is the best screening technique for LT wafers. A baseline reflection is made of the weak probe beam before the pump beam arrives from the unexcited semiconductor; this amplitude is denoted in Figure 27. When the pathlength of the pump and probe are changed so that the beams arrive simultaneously at the sample, the reflection of the probe beam from the photoexcitated plasma rises sharply towards it peak. The decay of the carriers is then

monitored by viewing the reflected probe-beam amplitude as the pump beam arrives earlier and earlier relative to the probe. The temporal resolution is very good due to the ≈100-fs duration optical pulses from a CPM dye laser.

To quantify and compare the recombination times, a curve has been fit to the decreasing side of the response curves, as shown by the dashed lines in the figure. This curve is hyperbolic, as justified by Mather et. al.,[4] where an extra offset has been added for the persistent transient reflectivity caused by thermal and diffusive effects. The estimate for the recombination time is given by the inverse of m^2 in the curve-fit expression (18 ps). Time-resolved reflectivity data generally overestimates the recombination lifetime obtained from photoconductively switched coplanar electrodes. For Sample 3-1251, this was true, yielding 12.5 ps with the photoconductive technique.

Photoconductively Switched Coplanar Electrodes

The second method of optical test used by the Ultrafast Science Laboratory involves coplanar electrodes that are photoconductively switched. A 15-μm gap switch (biased at 15V) is defined in a coplanar stripline with a characteristic impedance of 73Ω. *External electro-optic sampling* using a $LiTaO_3$ microprobe, and a CPM dye laser producing 100 fs optical pulses is used to measure the ultrafast switch response.[5] Figure 28 compares the measured responses for x=0.25 layers. Tables I and II also show the carrier lifetimes and responsivities of the various epilayers, as obtained from the above measurement. Growth temperatures in the range of 120-160°C produced single picosecond carrier lifetimes. Annealing, in general, improves the responsivity while degrading the lifetime. (Oscillations in the measured data are caused by reflections within the e-o probe.)

MSM Photodectors

To increase responsivity as a photoconductive detector, the electrode spacing can be reduced if the resistivity of the epilayer is high enough to sustain practical voltage levels.[2] Our MSM detectors were fabricated by hybrid lithography on wafers 3-1714 and 3-1751, the wafers with the shortest recombination times for x=0.25 and x=0.35. Our first procedure defined a 10mm-long coplanar stripline (necessary for the electro-optic sampling measurement) with contact lithography, and lifting off 500Å/2500Å, Ti/Au metallization. The detectors, which have an area of

13.5x21μm^2, were next placed in the center of this transmission line. To create the fingers of the MSM structure, we used 30 kV electron-beam lithography in 4000Å of PMMA resist. Ti and Au with thicknesses of 300 and 1200Å, respectively, were also used for the finger metallization. Detectors with 0.2, 0.5, 1, and 2μm finger widths and spaces were fabricated to compare speed and responsivity as a function of device geometry. Although pattern definition of the narrow finger devices on Sample 3-1714 was difficult due to a high density of misfit dislocations on wafer surface, there were no breaks in the electrical continuity of the 0.2 or 0.5μm fingers. The amorphous $In_{0.35}Ga_{0.65}$ As material of wafer Sample 3-1751 had a very smooth surface that was much more compatible with high-resolution lithography. Figure 29 shows a SEM photo of a 0.5μm MSM. Figure 30 shows the MSM detector responses for x =.25 material (Sample 3-1714), and Figure 31 shows the MSM detector responses for x=0.35 material (Sample 3-1751). The 1 ps of response at full-width half-maximum (FWHM) observed for the 3-1751 sample devices is the fastest measured speed for a long-wavelength photodetector. Here again, the oscillations in the responses are due to reflections within the electro-optic probe. The 0.2μm devices were not functional on the x=0.35 material, due to shorting of electrodes.

Further evaluation of the detectors is needed to completely understand their temporal behavior and responsivity. However, these general observations can be stated now:

1. The detectors on the 35% LT InGaAs have very poor responsivity, roughly a hundred times worse than the x=0.25 layer, consistent with the photoconductive switch data (Tables I and II), and presumably a result of the amorphous nature of the epilayer. The 25% LT InGaAs devices have responsivities in the 0.1 A/W range, comparable to LT GaAs.
2. The temporal responses of the 1- and 2-μm detectors are consistent with our photoconductive switch data presented in Tables I and II. However, the response slows down as the size of the electrodes is reduced, presumably due to increased capacitance since total detector area remains the same.

3. Although not included in the figures, detector response is sublinear with applied bias at low biases of <2V, probably due to some Schottky contact effects. We are trying to resolve this issue.
4. With reduced finger spacing and width, coupling of incident excitation light into the detector decreases due to diffraction effects, and hence an accurate measurement of actual light absorbed is needed to evaluate the responsivity accurately.

As Table II indicates, Sample 3-1748 exhibits one of the best combinations of a recombination time and responsivity. The recombination time of 4ps, although certainly not record-setting, is however slightly faster than the fastest InGaAs/InP PIN reported[6] and would provide a bandwidth over 100 GHz; also, its responsivity is one of the highest LT layers evaluated. Thus it offers an excellent compromise between speed and responsivity, being roughly four times slower than the devices made on sample wafer 3-1751, yet approximately 100 times more sensitive.

Data for Layers Grown in the Dislocation Reduction Study

For sample M-1331, pump-probe reflectivity and photoconductive switching have both been conducted on an as-grown section of the material, as well as on several chips that were annealed. A rapid thermal anneal was performed on pieces at temperatures of 600, 700, and 800°C, each for 30 seconds. Next, a metal pattern was established on the InGaAs in order to define a photoconductive gap to be used as a simple detector. This pattern also allowed determination of the sheet resistance of the material. The pattern consisted of two parallel lines on the top surface of the InGaAs, each 20 μm in width and with a 20 μm separation between them (coplanar stripline). The metalization was Ti-Au approximately 3000Å in thickness.

Our sheet resistance measurements were made with a DVM through leads that contacted the coplanar metal lines with tungsten probe tips positioned by an X-Y-Z translation stage. These reliably give us no more than a few ohms of contact resistance between the entire length of the lines, which were 1 cm long. As observed in Fig. 32, the resistance behavior of the LT-InGaAs has the same tendency as that of LT-GaAs – i.e., the as-grown material has a lower resistivity than the

annealed material - although in this case the resistivity is only one order of magnitude smaller for the as-grown sample, instead of the several orders of magnitude smaller typical for LT-GaAs. At the least, it appears that the trend of higher resistivity for the annealed sample is significant, since it was not unusual for the previously studied LT-InGaAs with dislocations to have a resistivity for the as-grown material that was 2-3 orders of magnitude higher than that for the annealed material. More samples should be studied to confirm this behavior in the LT-InGaAs on the buffers however. Also in comparison with LT-GaAs, the annealed M-1331 has a resistivity that is as much as several orders of magnitude lower than that expected for good-quality, annealed LT-GaAs. As far as the different RTA temperatures are concerned for M-1331, the sheet resistances vary between 1.25×10^7 and $1.7 \times 10^7 \Omega/\square$, with the suggestion of a saturation at the anneal temperature of 700°C. These values compare with a sheet resistance of the as-grown sample of 1×10^6 $\Omega/\square$ The resistance across the coplanar lines in each sample was not outstanding, but adequate for photoconductive switching to be performed.

As we have indicated in the past, the transient reflectivity characterization, while having higher temporal resolution, does not always yield results that are consistent with those acquired from photoconductivity, and sometimes negative tails or other polarity changes can not be explained. These may arise from optical effects, contributions to the index of refraction and the reflectance from phenomena other than photoexcited carrier populations, or the use of photo energies somewhat greater than the bandgap energy. The results of the transient reflectance experiment are shown in Fig. 33 for M-1331 samples as-grown and annealed at three temperatures. In each case the spot size for the pump beam was ~70μm diameter, and the 50-μm-diameter probe beam was focused inside the area of the pump beam. The pump and probe beams both had a photon energy of approximately 1.55 eV. The symbols on the experimental curves are markers intended only for identification purposes.

From the normalized reflectivity data, it was observed that the as-grown sample had a longer relaxation ($\tau_{1/e}$ ~13 ps)than any of the annealed samples, where the latter all had nearly the same $\tau_{1/e}$ of about 5 ps. The relaxation behavior of each seemed to follow a single exponential decay, although the reflectivity signals of the annealed samples decrease to levels slightly below those of persistent tails which

have amplitudes less than 5% of the peak reflectivity amplitude. This data is not consistent with our previous observations on LT-GaAs samples, which typically show as-grown material to have a shorter (albeit sometimes only slightly) lifetime.

The anomalous behavior of the relaxation time of the LT-InGaAs is by no means understood. It is reasonable to assume that only point defects, mostly due to excess arsenic, are present in the as-grown portion of the sample, and that arsenic precipitates that cause a decrease in the point defect density are present in the annealed materials. This suggests that the response of the material with the precipitates is faster than that of the material with only the point defects. Since the LT-InGaAs response differs so much from the usual temporal response of the LT-GaAs, one can initially speculate that perhaps there is some trapping/recombination center other than the EL2-like defect present in LT-GaAs.

The photoconductive switching measurement unfortunately contradicts the trends of the pump-probe relaxation data, in that the relaxation of the photogenerated carriers is faster for the as-grown material than for the annealed material (Fig. 34). (Four versions of Fig. 34 are provided, two with 10-ps windows (34a,b) and two with 40-ps windows (34c,d), one each normalized and one un-normalized.) The photoconductive switching takes place when a 25-mW beam illuminates the gap between the coplanar stripline. A dc-bias of 10 V is applied across the distributed gap, and the switched electrical transients are measured using an external electro-optic sampling probe. The photoconductive transients all display an exponential-like decay, although it is difficult to determine whether there are one or two components to the decay for all of them, due to the presence of a reflection at the time interval between 10 and 15 ps (in Fig. 34b, for example). This reflection is due to the electro-optic itself, and it cannot in all measurements be eliminated, depending on the geometry of the experiment. In Fig. 34a, it appears clear that the as-grown response is a two-component exponential. A 1/e decay can be identified after about 2 ps. The decay of the RTA sample at 600°C is about 5 ps, closely matching that measured in the transient reflectivity work. The next fastest decay is from the RTA

sample at 800°C (about 11 ps), followed by the 700°C RTA sample (15 ps). More measurements, perhaps at different fluence levels values, need to be performed to better understand the behavior observed in this experiment.

In this photoconductivity characterization, we have noted that the relaxation of the LT-InGaAs has a trend similar to that of LT-GaAs, in that the relaxation time of the as-grown material is shorter than for the annealed samples. M-1331 does act much more like LT-GaAs grown at temperatures somewhat above the optimum temperature of 200°C, however, since long-lived tails on the response are present.

It is unusual for the transient reflectivity and photoconductive measurements to behave in an opposite fashion such as this. It confuses any explanation of trapping/recombination mechanisms, and contributes to the uncertainty surrounding the physics and potential application of LT-InGaAs materials. Continued measurements on this and other samples are planned and will hopefully explain the inconsistencies. Table V tabulates the data for M-1331-34.

The table headings are defined as follows:

R(Ω) = is the actual resistance between coplanar striplines that were ~20 μm apart and about 1 cm long. It has not been reduced to sheet resistance or an estimate for resistivity.

Table 5. Electrical and Optical Test Data

		R(Ω)	(1/e) P.P. (lifetime) (ps)	(1/e) P.C. (lifetime) (ps)	Switching Efficiency	Tail**
M-1331	as-grown	3KΩ	~12ps	2.04ps	2.336/10=23.4%	7.6%
	600°C/30s	30KΩ	~5ps	5.04ps	16%	8.6%
M-1333	as-grown	1.4KΩ	?	1.46ps	5.8%	5.9%
	600°C/30s	N/A	N/A	N/A	N/A	N/A
M-1334	as-grown	3KΩ	6.89ps	3.10ps	11.0%	9.7%
	600°C/30s	23KΩ	4.07ps	~10ps	29.3%	17.3%

* Note that error bars could be a factor of 2 for these values. Responsivity would be the preferred figure of merit.
** At minimum decreasing slope.

JMB 3/9/94-3

P.P. = pump probe experiment. The lifetimes are 1/e times of the exponential decay.

P.C. = photoconductive-switching measurement, again with 1/e times.

Switching efficiency = the peak voltage we have measured divided by the DC voltage bias. Depending

on how a detector/switch would be used, the significance of this number can vary. If one is interested in photocurrent, then the responsivity is much more important, plus one has to be aware that a low resistance will lead to a high dark current. When we make our time-resolved photoconductive switching measurements, we look at electric field (of voltage), the variation of which can be rather large regardless of the dark current. However, if one wants to switch a large field or voltage, then a high efficiency is definitely important. The error bars can be large due to a number of factors, including the position of the focused laser beam on the switch.

"Tail" = the persistent photoconductivity as a percentage of the peak switched voltage. We try to estimate the tail level at a point where the slope is very small, and as such this is a qualitative measure of the contribution of the slowly varying part of the carrier relaxation. The question mark at the bottom of the column means that at the largest time window we could access, the slope was still decreasing appreciably.

M-1333 after RTA has not yet been characterized via photoconductive switching, mainly because we have measured many of these LT-InGaAs samples in the past.

The lifetime from the pump-probe reflectivity was longer in the as-grown LT-InGaAs on the graded buffer (M-1334) than for the annealed sample. On the other hand, the photoconductive lifetime was shorter in the as-grown sample than the annealed one. This is consistent with what we saw on M-1331.

Probably the most significant results of this dislocation reduction study is the virtual equivalence of PC lifetimes for InGaAs full of dislocations versus InGaAs that is free of dislocations, supporting the view that LT-induced defects, not dislocations, are responsible for short lifetimes. This is consistent with the trend of Table I, showing the decrease in lifetime as substrate temperature is reduced. (We saw no variation in dislocation densities or structure with reduced temperatures for samples in Table I). Another significant and related result is the higher switching efficiency realized in the dislocation-free material, consistent with the higher electron mobilities (Table III), and a benefit to applications requiring higher responsivity detectors.

Conclusion

LT $In_xGa_{1-x}As$ (x=0.25 –0.35) grown on GaAs has excellent promise as a photodetector in the 1.0-1.3μm range. The device so produced is integratable with other GaAs devices, giving it a great advantage over InP-based PINs. As with LT GaAs, the resistivity is generally higher after a brief anneal at 600°C, coinciding with the formation of As-rich precipitates. Also, as with LT GaAs, the lifetime shortens as the growth temperature is reduced; and the lifetime in LT $In_xGa_{1-x}As$ is generally shorter in as-grown samples than in annealed samples. To improve the crystalline quality and to distinguish detector speed and responsivity limitations due to dislocations versus defects induced by LT growth, we grew 3μm-thick graded layers of $In_xAl_{1-x}As$ between the GaAs substrates and $In_{0.35}Ga_{0.65}As$ films. The $In_xAl_{1-x}As$ layers are heavily dislocated, with the dislocation density increasing with distance from the GaAs substrate, and abruptly terminating at or below the $In_{0.35}Ga_{0.65}As$ layer. The resulting $In_{0.35}Ga_{0.65}As$ films are generally free of dislocations and electron mobilities are an order of magnitude higher than those of films grown directly on GaAs. Ultrafast optical testing using photoconductively switched coplanar electrodes show equivalent electron lifetimes of 1-3ps for dislocation-free LT $In_{0.35}Ga_{0.65}As$ and LT $In_{0.35}Ga_{0.65}As$ grown directly on GaAs, demonstrating that the short electron lifetimes are caused by LT-induced defects. This correlates with the trend reported by us previously for LT $In_xAl_{1-x}As$ grown directly on GaAs, namely that the electron lifetime decreases with decreasing growth temperature, as also observed for LT GaAs.

References

1. S. Gupta, M. Frankel, J.A. Valdmanis, J. Whitaker, G. Mourou, F.W. Smith, and A.R. Calawa, *Appl. Phys. Lett.* 59 (25), 3276 (1991).
2. Y. Chen, S. Williamson, T. Brock, F.W. Smith, and A.R. Calawa, *Appl. Phys. Lett.* 59 (16), 1984 (1991).
3. F.W. Smith, Ph.D. Thesis, Massachusetts Institute of Technology, (1990).
4. V.K. Mather, P.S. Mak, and C.H. Lee, *J. Appl. Phys.* 51 (9) (September 1980).
5. J.A. Valdmanis, *Electron Lett.* 23, 1310 (1987).
6. Y.G. Wey et.al., *Appl. Phys. Lett.* 58, 2156 (1991).

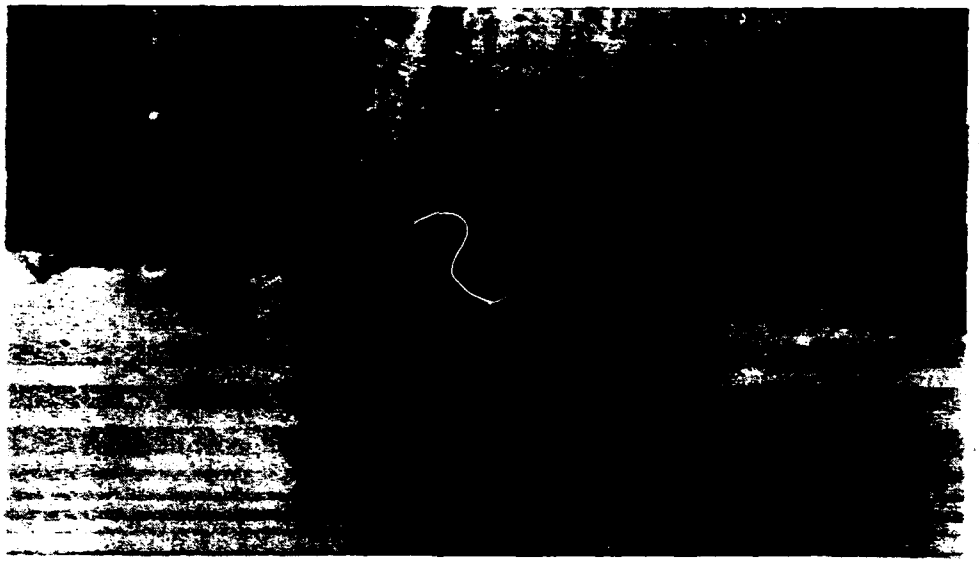

40000X

Figure 1. TEM Cross-Section of 3-1626, Grown at 200°C and Annealed, is Representative of x=0.25 Layers Grown in the 200-300°C Range and Annealed

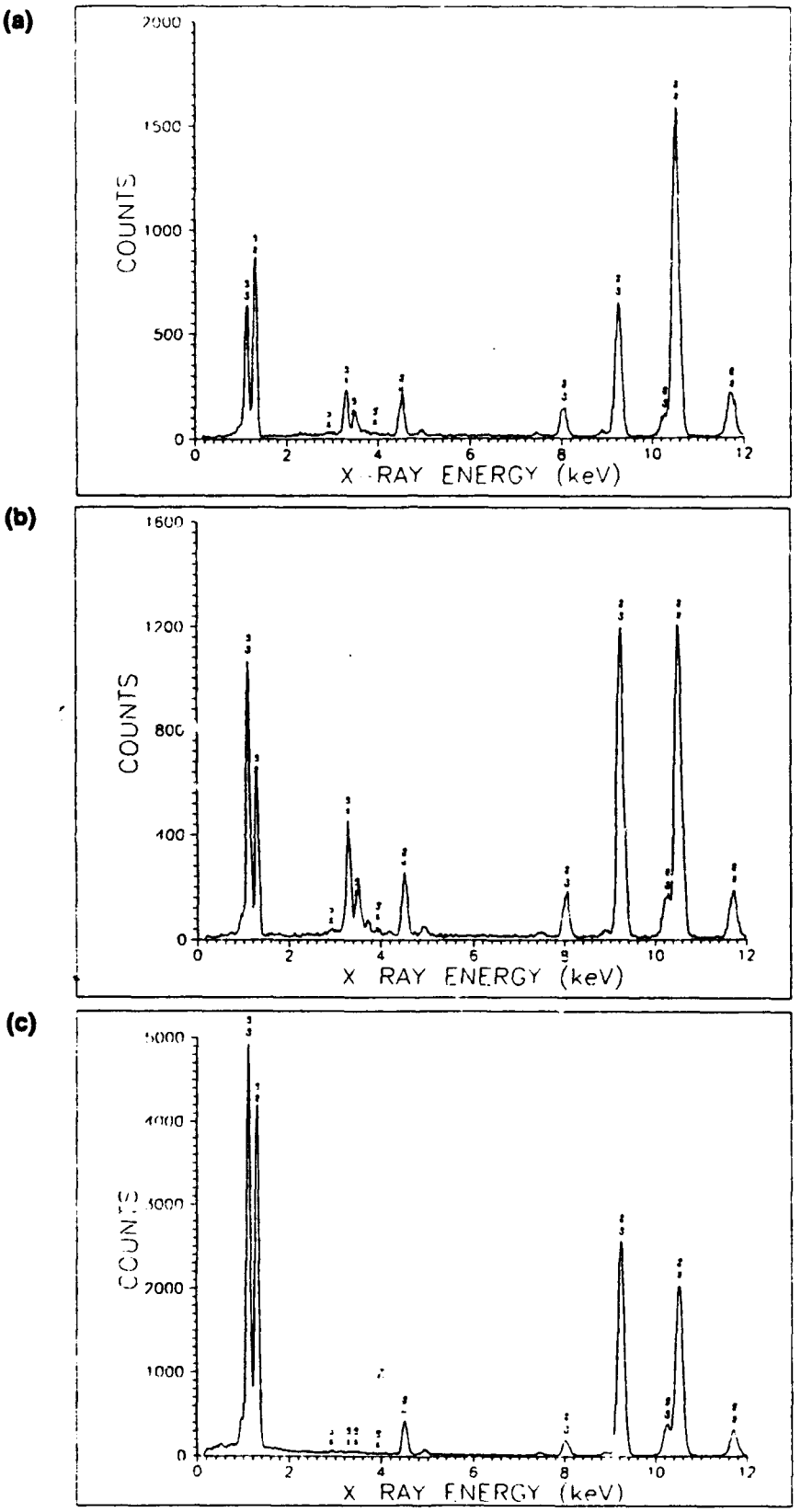

Figure 2. Energy Dispersive X-ray Data Taken from the Electron Beam Positioned in Three Different Areas of 3-1626 (a) on a Precipitate, (b) on the InGaAs Matrix Near a Precipitate, and (c) on the GaAs Substrate

41000000X

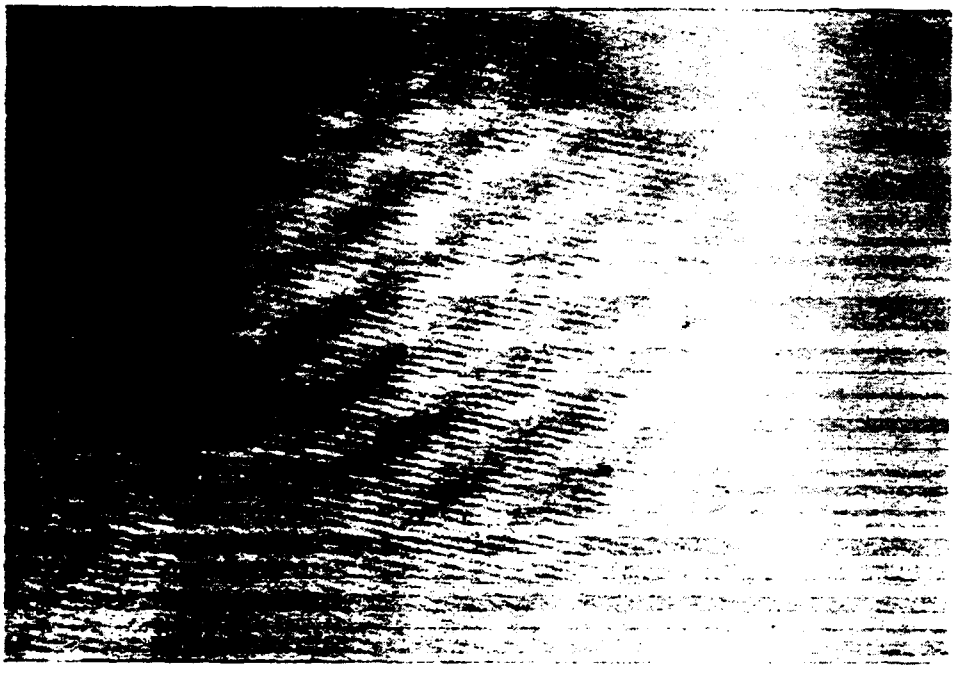

80000000X

Figure 3. High Resolution Imaging of Two Precipitates in 3-1626

90000X

Figure 4. TEM Cross-Section of 3-1713, Grown at 160°C, Showing Microtwin Defects Residing Along <111> Planes

190000X

Figure 5. TEM Cross-Section of 3-1714, Grown at 160°C and Annealed

Figure 6. TEM Electron Diffraction Patterns Show Characteristic Twin Spots from the Macroscopic Domains in 3-1714

190000X

Figure 7. Large Precipitates Are Visible in This TEM Cross-Section of 3-1714

150000X

Figure 8. TEM Cross-Section of 3-1747, x=0.35 Grown at 200°C

90000X

Figure 9. TEM Cross-Section of 3-1749, x=0.35 Grown at 160°C, is Predominantly Amorphous, But Exhibits Small Polycrystalline Domains in the Surface Region

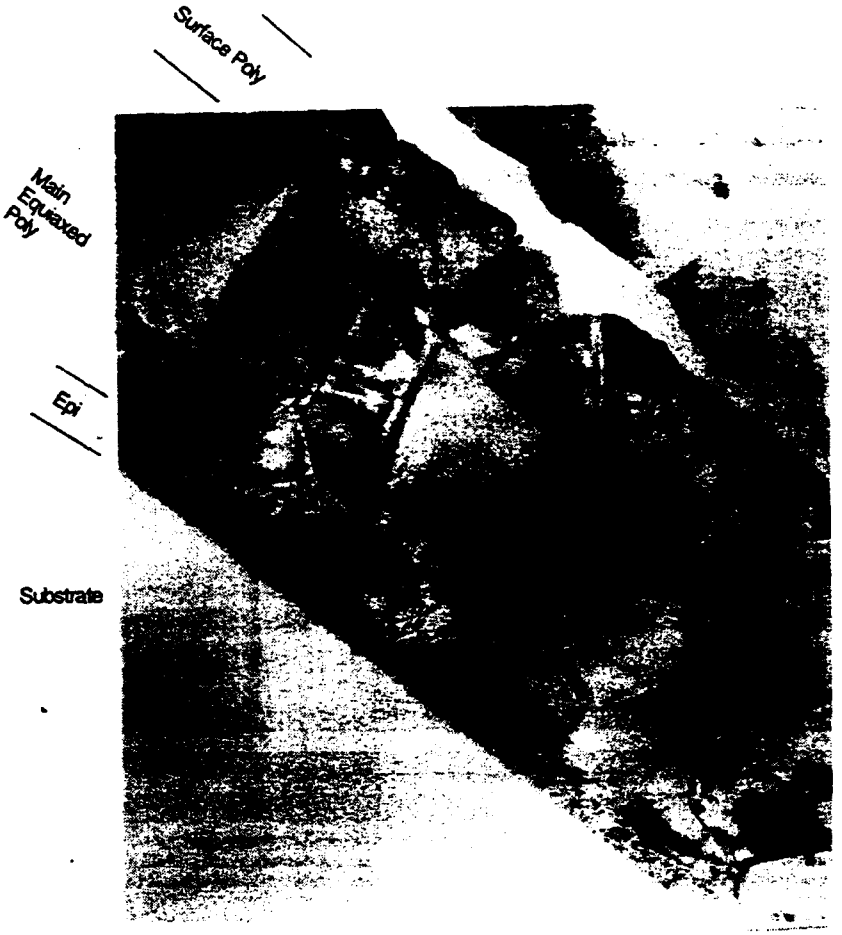

90000X

Figure 10. TEM Cross-Section of 3-1750, x=0.35 Grown at 160°C and Annealed, Exhibits Three Regions—A Near Substrate Epitaxial Region, a Large Equiaxed Grain Center Region, a Small Equiaxed Grain Near Surface Region

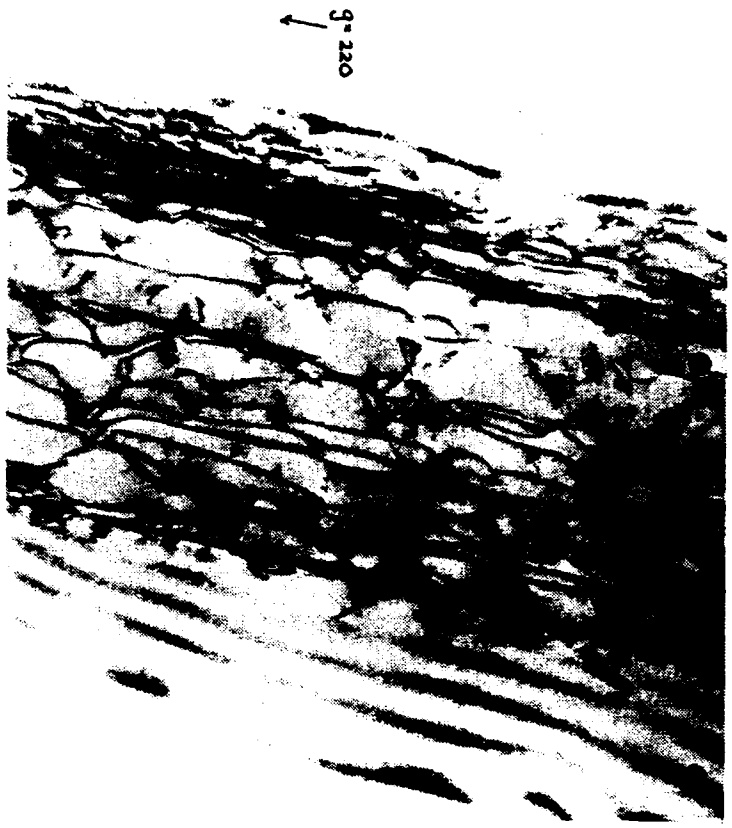

52500X

Figure 17. TEM Cross-section of M-1331 Taken With Diffracting Vector g=220

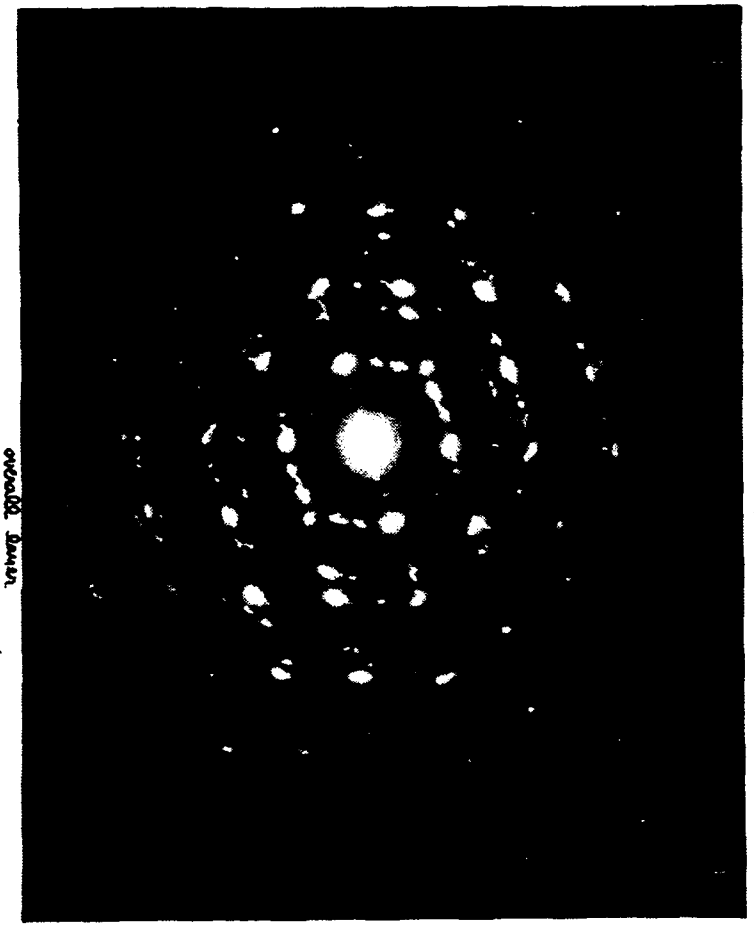

Figure 18. Diffraction pattern of M-1333, $In_{0.35}Ga_{0.65}As$ Grown Directly on GaAs. Twins are present at a very high density.

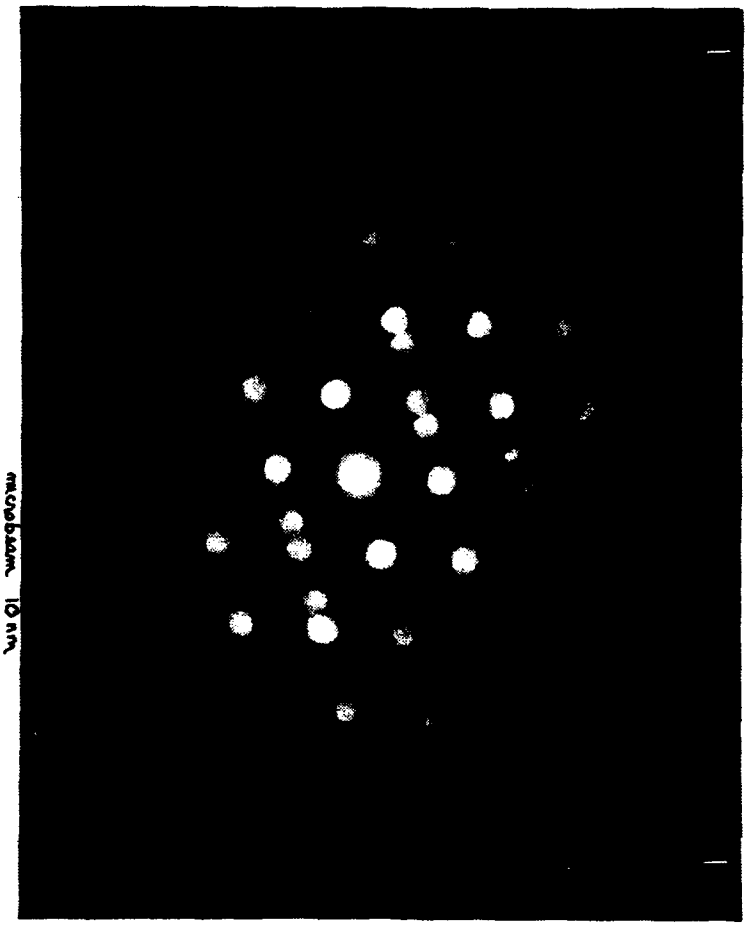

Figure 19. Microdiffraction Pattern for ~10nm Domain Within M-1333, Indicating Twinning on (111) Plane.

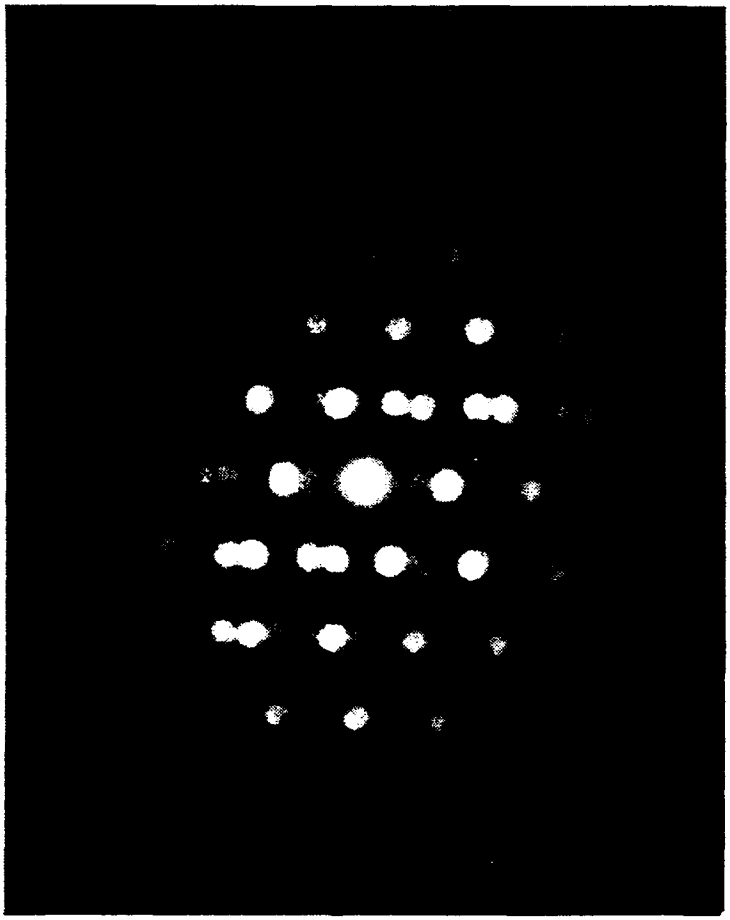

Figure 20. Microdiffraction Pattern for ~10nm Domain Within M-1333, Indicating Twinning on (-1-11) Plane, Mirror to (111).

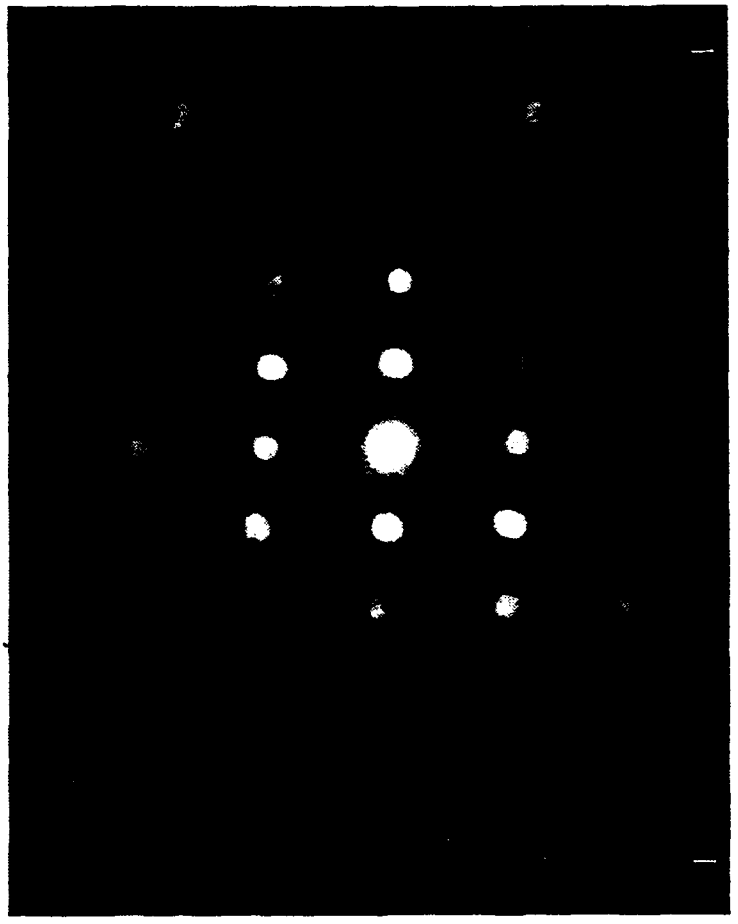

Figure 21. Microdiffraction Pattern for ~10nm Domain Within M-1333, oriented with a {211} normal which is not epitaxial.

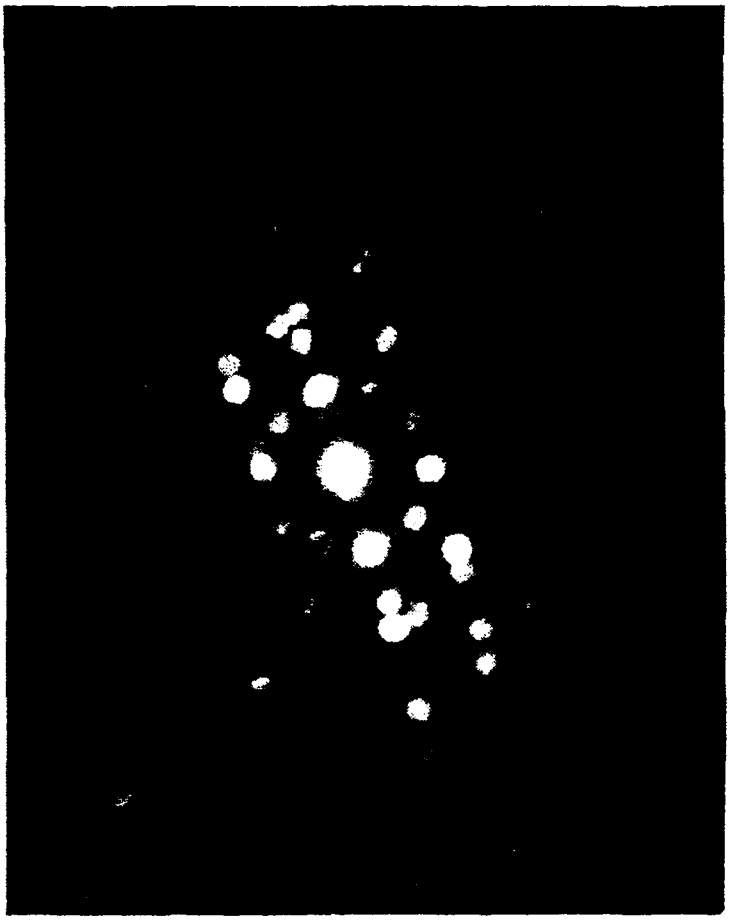

Figure 22. Microdiffraction Pattern for ~10nm Domain Within M-1333, showing multiple twinning in a small region.

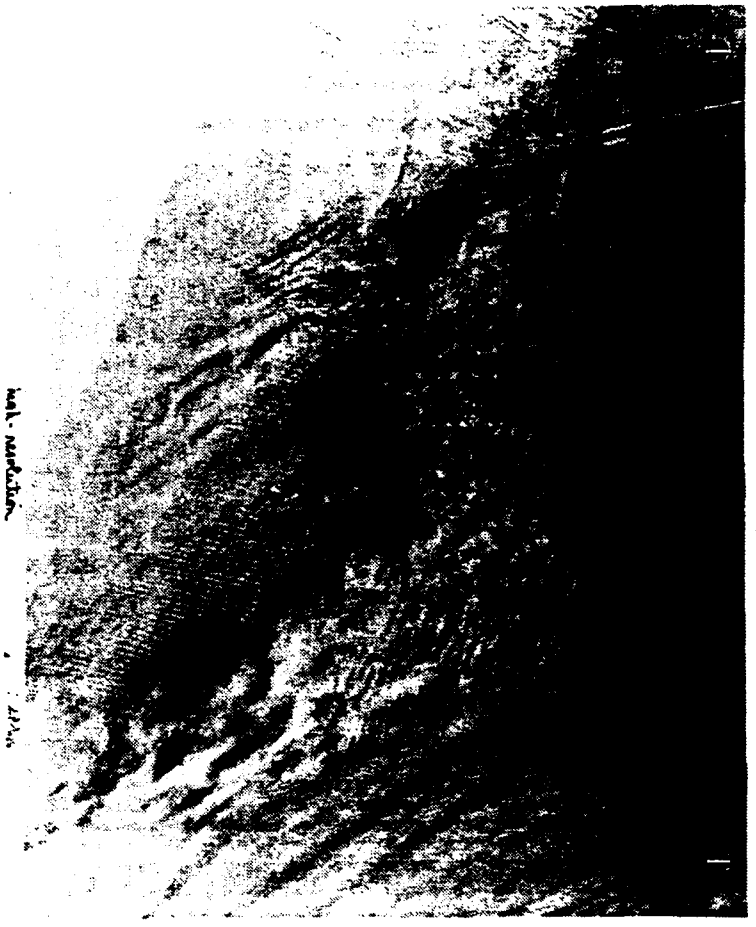

1200000X

Figure 23. High Resolution TEM Cross-Section of M-1333, Showing Heavily Defective Nature of Crystal on Small Scale.

1200000X

Figure 24. High Resolution TEM Cross-Section of M-1333, Showing Heavily Defective Nature of Crystal on Small Scale.

42000X

Figure 25. TEM Cross-Section of M-1334, Showing Similar Results to That of M-1331 (Fig. 11), Though Here Defects Appear in the Dislocation-free Zone in the Top ~0.2μm of InAlAs.

30000X

Figure 26. TEM Cross-Section of M-1334, Showing Some Evidence of Strain in the InGaAs Near the Faults Extending Through the Dislocation-free Zone of InAlAs.

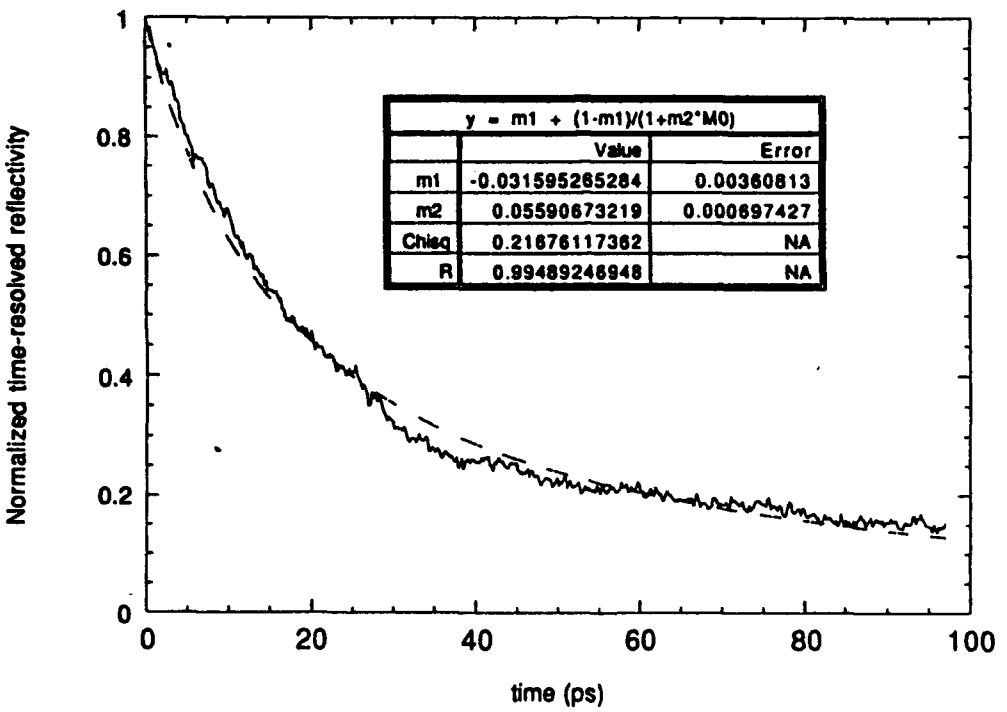

Figure 27. Time-Resolved Reflectivity Scan of 3-1251, x=0.25 Grown at 300°C, Shown Here to Illustrate the Technique

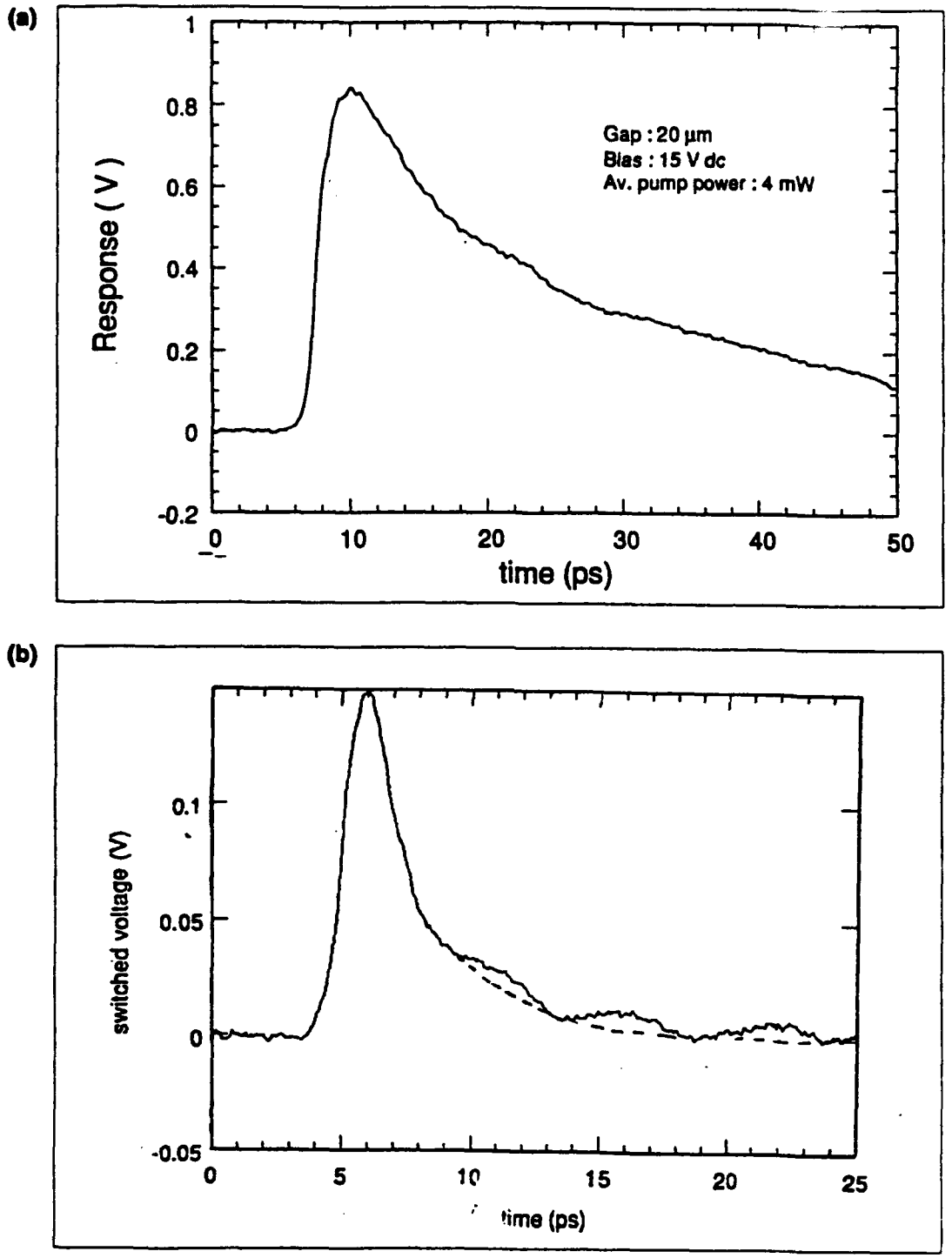

Figure 28. Photoconductively Switched Coplanar Electrode Results for 3-1252, x=0.25 Grown at 300°C and Annealed, and 3-1714, Grown at 160°C and Annealed

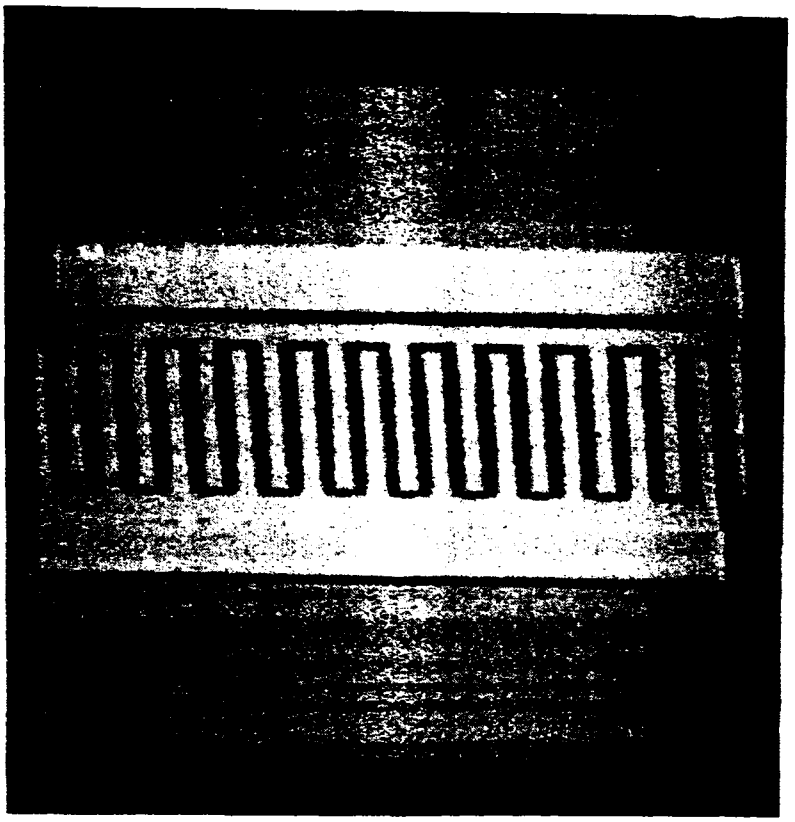

Figure 29. SEM Photo of MSM Photodetector with 0.5μm Finger Widths and Spacings

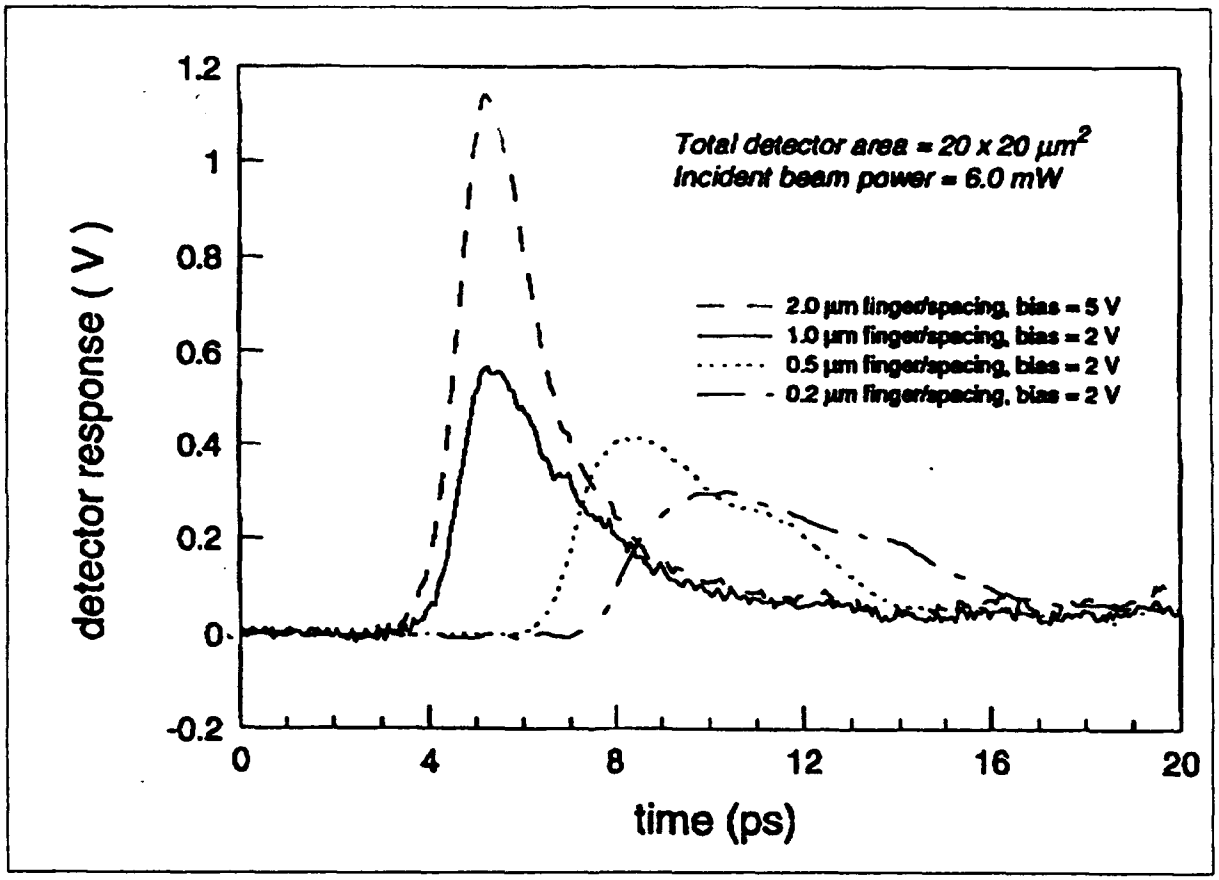

Figure 30.MSM Detector Results for 3-1714, x=0.25 Grown at 160°C and Annealed

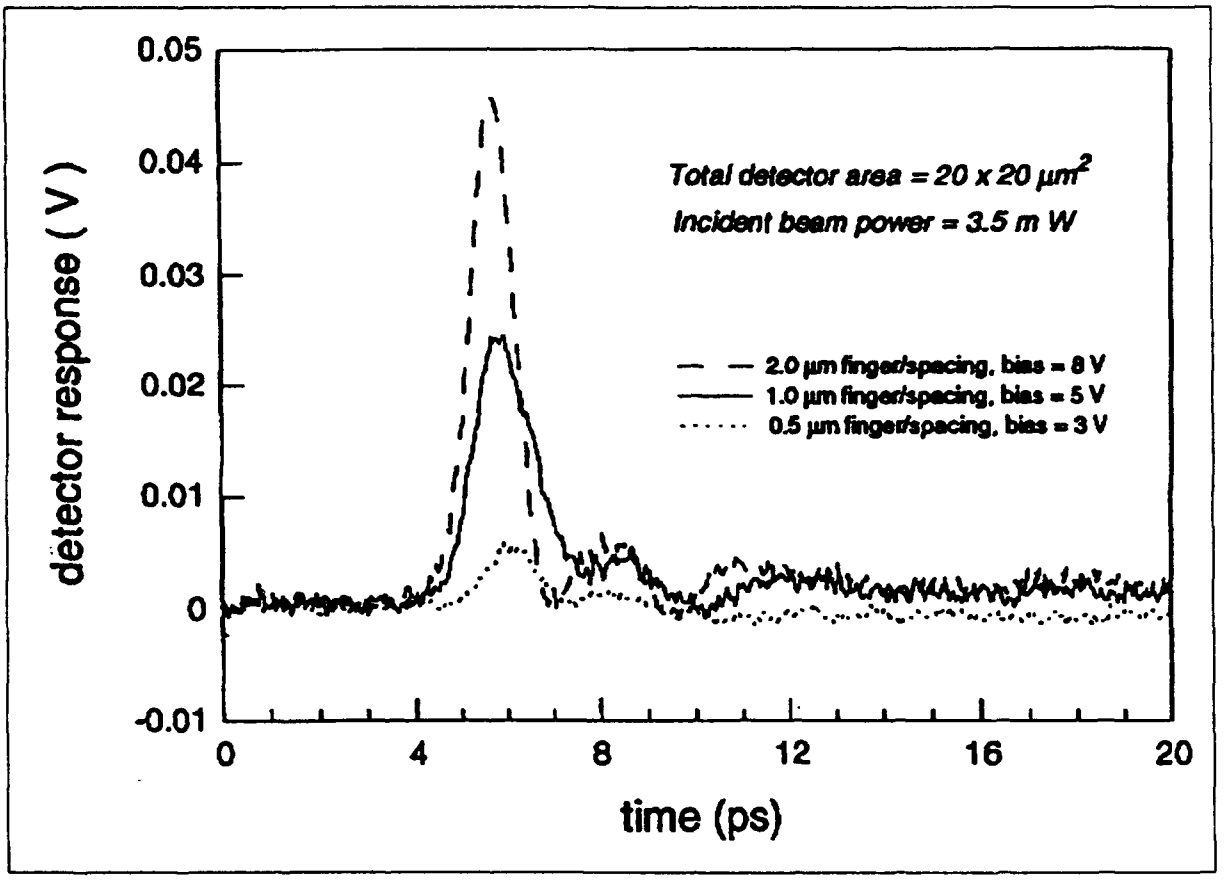

Figure 31. MSM Detector Results for 3-1751, x=0.35 Grown at 120°C

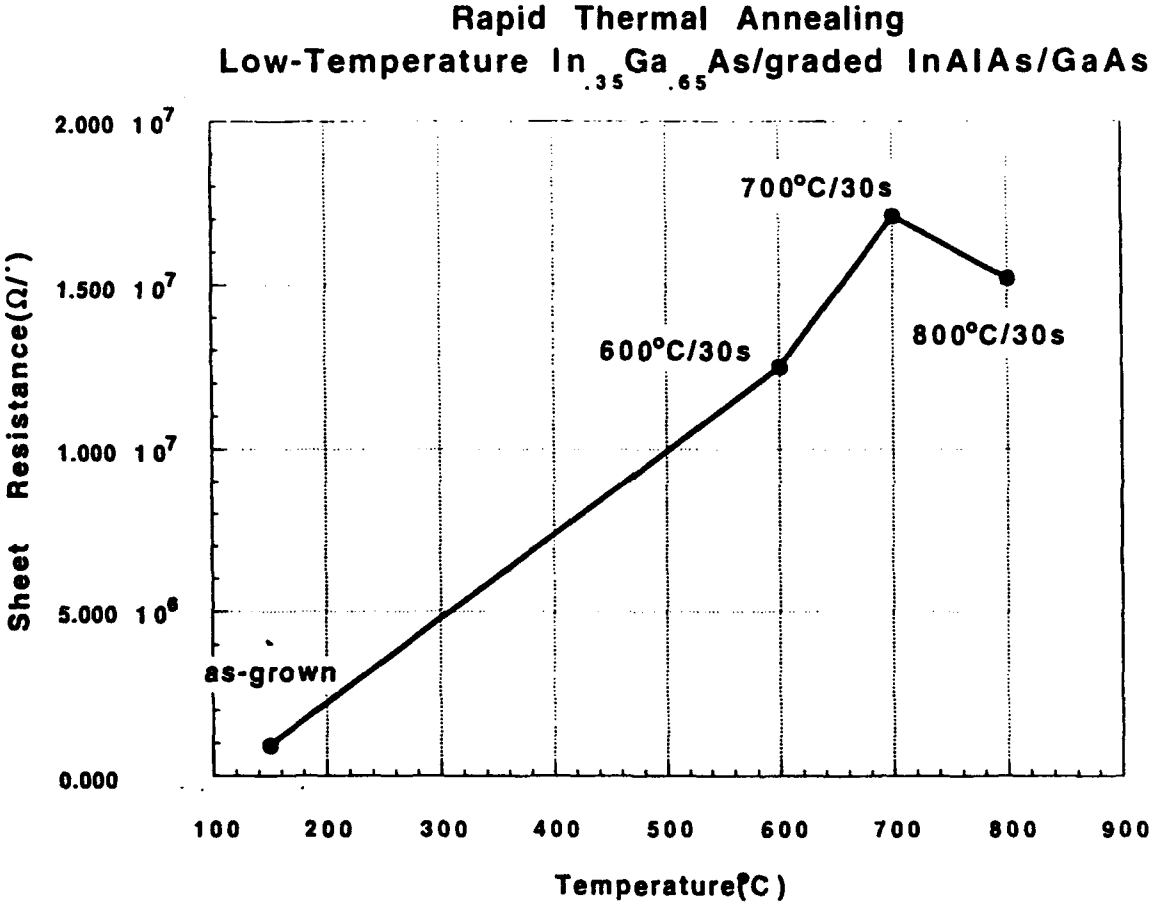

Figure 32. Sheet Resistance of M-1331 for As-grown Material and Rapid Thermal Annealed Material

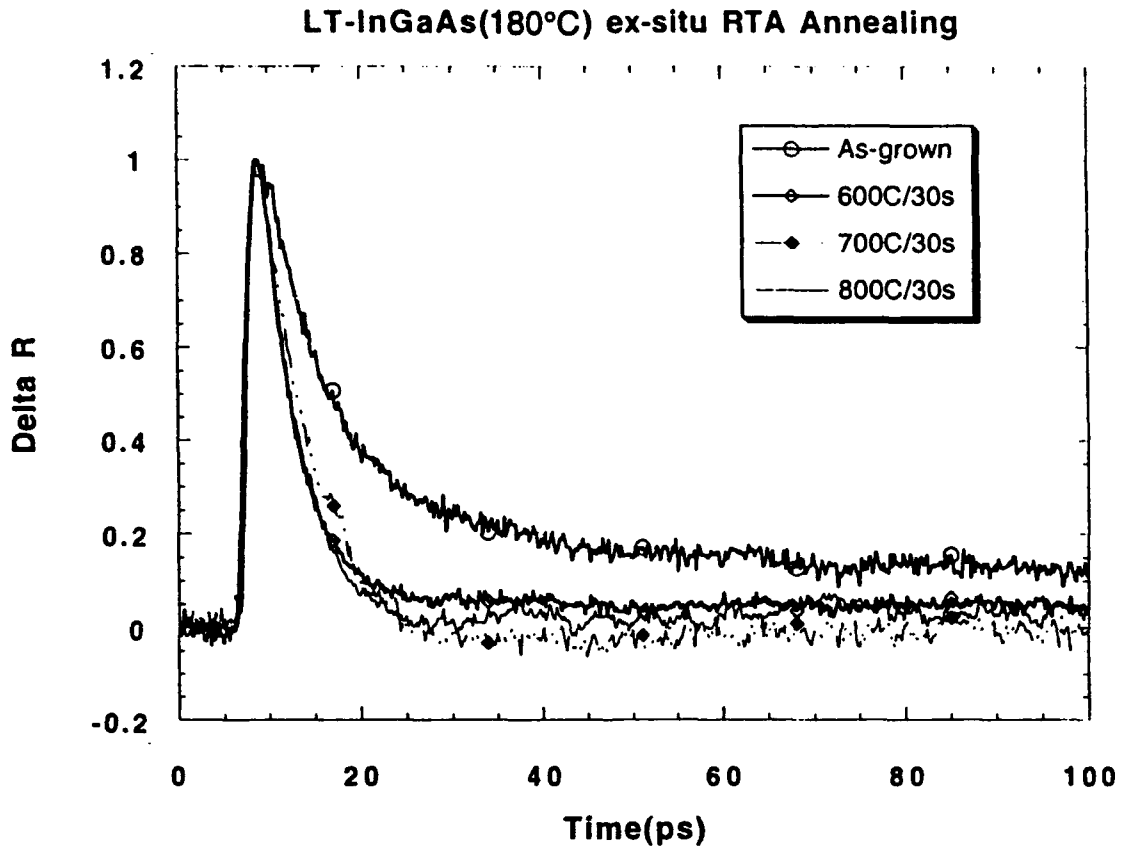

Figure 33. Transient Reflectance data for M-1331, As-grown and Annealed Samples.

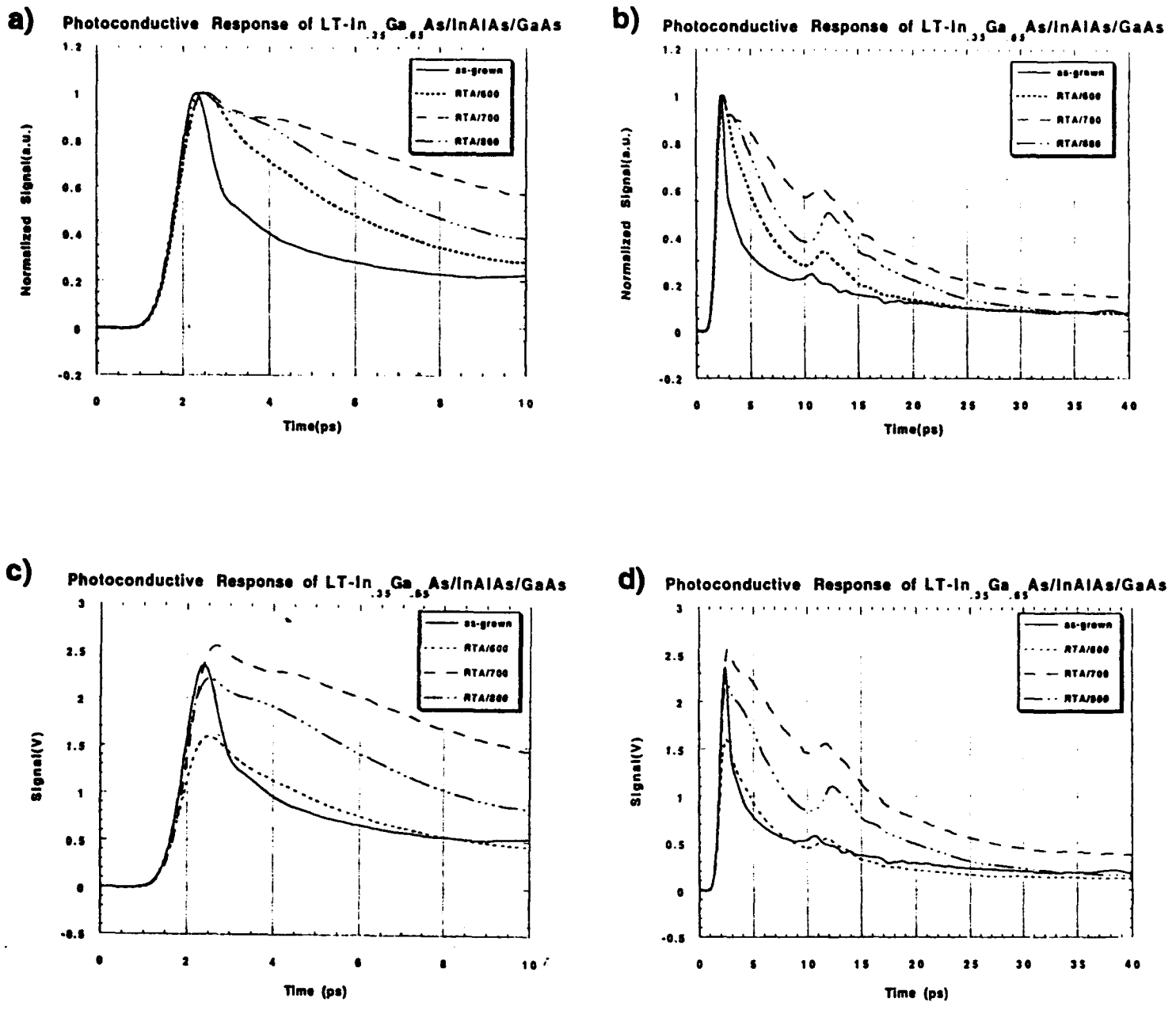

Figure 34 (a-d). Photoconductive Response Data for M-1331, As-grown and Annealed Samples